Journal of the European Ceramic Society 22 (2002) 2389–2400

www.elsevier.com/locate/jeurceramsoc

Microstructural and mechanical characterization of sol gel-derived Si–O–C glasses

S. Walter[a,1], G.D. Soraru[a,*], H. Bréquel[b], S. Enzo[b]

[a]*Università degli Studi di Trento, Ingegneria dei Materiali, Via Mesiano 77, I-38050 Trento, Italy*
[b]*Università degli Studi di Sassari, Dipartimento di Chimica, I-07100 Sassari, Italy*

Received 17 August 2001; received in revised form 22 November 2001; accepted 8 December 2001

Abstract

The mechanical properties of three silicon oxycarbide glasses pyrolysed under inert (Ar) atmosphere were studied as a function of the pyrolysis temperature. The silicon oxycarbide glasses were prepared from various alkyl substituted alkoxysilanes such as $HSi(OEt)_3$ and $HMeSi(OEt)_2$ in different ratios by using the sol-gel method. The Si–O–C-glasses obtained were respectively: (i) silicon oxycarbide network with excess carbon, (ii) stoichometric $SiC_xO_{2(1-x)}$ where $x=0.30$ and (iii) silicon oxycarbide matrix with an excess of Si. Si–C bonds introduced in the starting silica gel network can be partially retained in the final glass after pyrolysis under inert atmosphere. After pyrolysis at temperatures between 600–1500 °C, the presence of tetracoordinated C atoms in the silica network results in an improvement of mechanical properties and thermal stability compared with silica glass. By using elemental analysis, density, SEM, BET and XRD (combined with Rietveld-analysis), the glass characterization was performed. Flexural strength (*MOR*), elastic modulus (*E*) and Vickers hardness (H_V) were measured and will be discussed in terms of glass composition and microstructure. © 2002 Published by Elsevier Science Ltd.

Keywords: Glasses; Mechanical properties; Microstructure-final; Si–O–C; Sol-gel processes

1. Introduction

Ceramic materials are widely used in various fields not only for their good mechanical performances with respect to low density, but also for the range of optical, electrical and magnetic properties they can cover. Some of the properties of such advanced materials may be selected and optimized by an accurate control of their composition and microstructure. For the development of applications at increased temperatures, considerable efforts are made in the production of materials with improved mechanical properties and heat resistance. This led over the last several years to the elaboration of advanced ceramics with complex shapes like fibers, coatings or matrices for ceramic matrix composites, CMCs. In the case of silica glass, efforts are made mainly to increase high temperature mechanical properties and devitrification resistance through substitution of oxygen by carbon atoms in the amorphous network, leading to novel silicon oxycarbide glasses.[1]

The sol-gel process is an attractive synthetic approach to produce silicon oxycarbide glasses, as revealed by the number of studies published in this field.[2–4] Organically modified alkoxysilanes ($R_xSi(OR')_{4-x}$, $x=1, 2$; $R=H$, CH_3, CH_3CH_2, $CH_2=CH\ldots$; $R'=CH_3$, CH_3CH_2), that are molecular precursors containing Si–O and Si–C bonds, can be hydrolyzed and condensed without decomposition or loss of the carbon functional groups, leading to hybrid silica-based gels. The pyrolysis of such gels above 1000 °C under inert atmosphere leads to SiOC glasses. The pyrolysis product can be expressed as $SiC_xO_{2(1-x)}+yC_{free}$, where $SiC_xO_{2(1-x)}$ describes the composition of the amorphous oxycarbide network and yC_{free} the amount of carbon, typically present as a secondary free carbon phase. The silicon oxycarbide network is formed by a random array of SiC_zO_{4-z} units ($0\leqslant z\leqslant 4$)[5] and carbidic carbon CSi_4 unit.

Compared to the parent silica glass, the presence of tetracoordinated carbon units leads to a stiffer and

* Corresponding author. Tel.: +39-461-882-454; fax: +39-461-881-977.

E-mail addresses: soraru@ing.unitn.it (G.D. Soraru), steffen.walter@mchp.siemens.de (S. Walter).

[1] Present address: SIEMENS AG, CT MM2, Ceramics Department, Otto-Hahn-Ring 6, 81730 Munich, Germany.

0955-2219/02/$ - see front matter © 2002 Published by Elsevier Science Ltd.
PII: S0955-2219(01)00537-4

constrained network with improved mechanical properties such as elastic modulus (E), flexural strength (MOR) and hardness as well as density, viscosity and glass transition temperature.[6] The carbon containing network has a lower tendency toward devitrification[7] and it is evident that silicon oxycarbide glasses can be used as a modification of SiO_2 glass for high temperature application, when the use of silica is limited due to its devitrification or low viscosity, which results in high creep rates.

In our laboratory, we are able to synthesize monolithic silicon oxycarbide glasses, starting from gel precursors containing Si–CH_3 and Si–H groups.[8] These monolithic gel samples were pyrolysed at temperatures between 1000 and 1200 °C to measure mechanical properties (elastic modulus, flexural strength or Vickers hardness) of the amorphous silicon oxycarbide phase.[9,10] It was clearly demonstrated that the C-incorporation in the silica network increases the mechanical properties: E values up to 110 GPa and MOR values up to 700 MPa were reported.

The objective of the present paper is to follow a systematic characterization of the mechanical properties depending on the phase composition of three silicon oxycarbide glasses as a function of the pyrolysis temperature between 600 and 1500 °C. This temperature range embraces three important areas for polymer derived oxycarbide glasses:

1. bond cleavage (600–1000 °C): cleavage of Si–H, Si–C and C–H bonds leads to evolution of hydrocarbons and hydrogen and transforms the organic compound into an inorganic material (SiOC glass);
2. SiOC glass (1000–1200 °C): a random array of mixed silicon oxide units SiC_xO_{4-x} units ($0 \leqslant x \leqslant 4$) form an amorphous network;
3. phase separation (1200–1500 °C): SiOC glass separates leading to the precipitation of nanosized β-SiC and graphitic carbon clusters (C_{free}) embedded into an amorphous SiO_2,matrix.[11] A carbothermal reduction process to form gaseous products like SiO and CO is also common in this temperature range.[12]

According to these temperature steps, the mechanical properties (MOR, elastic modulus, Vickers hardness) of the silicon oxycarbide glasses will be discussed in terms of glass composition (elemental analysis), phase composition (X-ray diffraction combined with Rietveld-analysis) and microstructure (density, BET, SEM).

2. Experimental procedure

Gels were prepared starting from triethoxysilane ($HSi(OEt)_3$, TREOS) and methyldiethoxysilane ($HMeSi(OEt)_2$, MDES) with ratios 1/1 (T^H/D^H1), 2/1 (T^H/D^H2) and 9/1 (T^H/D^H9). These compositions were choosen because, according to the literature[13,14] they are precursors for stoichiometric silicon oxycarbide glasses (T^H/D^H2), or with excess C (T^H/D^H1) or Si (T^H/D^H9). Ethanol was used as solvent (Si/EtOH = 1/2) and water acidified with HCl (pH = 4.5) to promote hydrolysis reactions ($H_2O/OR = 1/1$).

2.1. Preparation of monolithic samples for flexural tests

The solutions were cast into small plastic test tubes (having a diameter of 5 mm) and were left open for 5 weeks. Accordingly, monolithic gel rods (diameter 2.5 mm and length ≈30 mm) were obtained. Wet gels were dried in temperature steps (40, 60, 80, 100, 120 °C) for 2 days, respectively. Pyrolysis was carried out in a graphite furnace (Astro, Thermal Technologies Inc.) at temperatures between 600 and 1500 °C in Argon atmosphere. The firing treatments were performed with heating and cooling rates of 5 °C/min. Above 1000 °C, heating and cooling rates of 1 °C/min were necessary to prevent crack formation for T^H/D^H2 and 9 compositions. On the other hand, for T^H/D^H1 samples, even at 1 °C/min, it was not possible to process crack-free SiOC rods. For this reason the mechanical characterization by flexural tests was performed up to 1000 °C and no data are available for higher temperatures.

2.2. Preparation of monolithic samples for Vickers hardness tests

In this case the gelling solutions were cast into test tubes having a diameter of 10 mm. After gelling and drying, monolithic gel rods with a diameter of ≈6 mm were produced. From these samples, gel disks were obtained by sawing. The disks were subsequenty pyrolyzed with the same heating schedule as for the samples for flexural tests. Accordingly, SiOC discs ≈5 mm in diameter and 1.5 mm thickness were obtained and used for the subsequent indentation experiments.

2.3. Preparation of powder samples for microstructural characterization

In this case, part of the gel produced for hardness measurements was grinded and sieved to collect the fraction between 100 and 350 μm. Pyrolysis of these powders was performed as previously described.

2.4. Chemical analysis

Gel samples and the powder pyrolysis products were analysed for Si, C and H by the Service d'Analyse Elementaire du CNRS, France. Oxygen content was estimated by difference.

2.5. Flexural tests

Flexural tests were performed with 4-point bend loading geometry (20/10) using a MTS machine (Model 810) with a crosshead speed of 1 mm/min. Five samples (as pyrolysed) were tested for each composition and pyrolysis temperature. (*MOR*) was calculated from the standard equation for cylindrical samples:

$$\sigma_B = \frac{F_M \ 80}{\pi \ d^3} \quad (1)$$

where F_M is the maximum load and d the diameter of the rod. By measuring the displacement δ at any given load F, the elastic modulus E was also computed:

$$E = \frac{FD(3L^2 - 4D^2)}{48I\delta} \quad (2)$$

where L is the outer span (20 mm), D the inner span (5 mm) and $I = ((\pi d^2/64))$ the moment of inertia of the samples.

2.6. Vickers Hardness H_V

H_v was measured on surfaces polished with 3 μm diamond paste, using a micro indenter (Officine Galileo) with 10 N as indentation load and contact time of 15 s. The diagonals of the impression were measured using an optical microscope (Reichert Polyvart 2-MET).

2.7. Fractographic analysis

Fracture surfaces collected after *MOR* evaluation and cross-section of indents were studied by scanning electron microscopy SEM (Jeol JSM 6400). To prevent charging effects on the surface, samples were previously sputtered with a gold film (10 nm).

2.8. Microstructural characterization

Density measurements were performed using a He-pycnometer (Multivolume Pycnometer 1305, Micromeritics). Specific Surface Area (SSA) and pore size distribution were evaluated from nitrogen adsorption/desorption measurements 77 K using an ASAP 2010 (Micromeritics) instrument. SSA was determined from a BET (Brunauer, Emmet and Teller) analysis in the P/P_0 range of 0.05–0.30 using a molecular cross sectional area for N_2 of 0.163 nm^2 and a minimum of 5 data points. The pore size (radius) distribution was obtained from the desorption isotherm through the BJH (Barret, Joyner and Halenda) analysis.[15] X-ray diffraction patterns were collected with a Bragg-Brentano powder diffractometer using Cu$K\alpha$ radiation ($\lambda = 1.54178$ Å) and Mo$K\alpha$ radiation ($\lambda = 0.7103$ Å). The molybdenum source was used to cover a wider interval of scattering vector $S = 4\pi \sin\theta/\lambda$. A graphite monochromator was used in the diffracted beam. The data collection with Cu radiation was carried out from $2\theta = 6$–$145°$ with a step of 0.02° and an acquisition time of 10 s. With Mo beam source the angular range was the same but with a step of 0.2° in correspondence of the high angle weak features to gain better statistics. Diffraction data were analysed by the Rietveld method, using the fully automated code RIETQUAN,[16] particularly useful for a quantitative evaluation of phases and reliable structural and microstructural information such as unit cell, average crystallite size and lattice strain.

3. Experimental results

3.1. Microstructural characterization

From the elemental analysis of the gels and the pyrolysed silicon oxycarbide samples at temperatures between 400 and 1500 °C, the empirical formula was calculated and reported in Table 1. In the same table the composition of the silicon oxycarbide glass is expressed as $SiC_xO_{2(1-x)} + yC_{free}$ (or ySi_{free}) where $SiC_xO_{2(1-x)}$ describes the composition of the amorphous oxycarbide network and yC_{free} (or ySi_{free}) the amount of carbon (or silicon) forming a secondary phase. It can be useful to re-write $SiC_xO_{2(1-x)}$ as: $xSiC + (1-x)SiO_2$ and to observe that the x value in the silicon oxycarbide formula is a direct measure of the relative amount of Si–C and Si–O bonds present in the glass network.

Beginning from the composition of the gels, the C/Si ratio decreases with increasing T^H/D^H ratio of the precursors, while the O/Si ratio increases. With increasing pyrolysis temperature up to 1500 °C, each composition shows a decrease of the C/Si ratio and an increase of the O/Si ratio. Except fot T^H/D^H 1, hydrogen is bonded in the network up to 800 °C. At temperatures higher than 1000 °C, the selected compositions show the presence of mixed silicon oxycarbide units, $SiO_{4-x}C_x$ with $0 \leqslant x \leqslant 4$.[8] Pyrolysis of T^H/D^H 1 samples leads to oxycarbide materials with a C_{free} phase. T^H/D^H 2 compositions can be pyrolysed into an almost pure oxycarbide phase with very low amounts of excess C or Si. T^H/D^H y compositions with $y \geqslant 2$ lead to oxycarbide glasses with extra Si–Si bonds in the amorphous network, which reaches the maximum amount, for the T^H/D^H 9 precursor. The amount of bonded carbon, i.e. the x value in the formula: $SiC_xO_{2(1-x)}$ decreases from the T^H/D^H 1–9 composition.

The microstructural evaluation of the different oxycarbide glasses as a function of the pyrolysis temperature were performed by density measurements, SSA analysis as well as the pore size distribution and X-ray diffraction analysis.

Table 1
Empirical and stoichiometric compositions of the gels and corresponding oxycarbide glasses pyrolyzed in Ar (1 h) at temperatures between 400 and 1500 °C

Pyrolysis parameter	T^H/D^H 1		T^H/D^H 2		T^H/D^H 9	
	Oxycarbide glass composition		Oxycarbide glass composition		Oxycarbide glass composition	
	Empirical formula	Stoichiometry	Empirical formula	Stoichiometry	Empirical formula	Stoichiometry
Gel	$SiC_{0.53}O_{1.29}H_{2.49}$		$SiC_{0.35}O_{1.28}H_{1.93}$		$SiC_{0.24}O_{1.48}H_{1.48}$	
400 °C	$SiC_{0.40}O_{1.59}H_{1.48}$		$SiC_{0.32}O_{1.42}H_{1.38}$		$SiC_{0.12}O_{1.61}H_{0.84}$	
600 °C	$SiC_{0.43}O_{1.41}H_{2.51}$		$SiC_{030}O_{1.47}H_{0.72}$		$SiC_{0.12}O_{1.63}H_{0.38}$	
800 °C	$SiC_{0.40}O_{1.57}H_{1.05}$		$SiC_{0.28}O_{1.44}H_{059}$		$SiC_{0.13}O_{1.71}H_{0.26}$	
1000 °C	$SiC_{0.39}O_{1.38}H_{0.54}$		$SiC_{0.30}O_{1.49}$	$SiC_{0.26}O_{1.49}+0.04C$	$SiC_{0.14}O_{0.61}$	$SiC_{0.14}O_{1.61}+0.05Si$
1200 °C	$SiC_{0.38}O_{1.39}$	$SiC_{0.31}O_{1.39}+0.07C$	$SiC_{0.27}O_{1.49}$	$SiC_{0.25}O_{1.49}+0.02C$	$SiC_{0.12}O_{1.55}$	$SiC_{0.12}O_{1.55}+0.11Si$
1400 °C	$SiC_{0.35}O_{1.37}$	$SiC_{0.32}O_{1.37}+0.03C$	$SiC_{0.26}O_{1.41}$	$SiC_{0.26}O_{1.41}+0.04Si$	$SiC_{0.13}O_{0.13}$	$SiC_{0.13}O_{1.53}+0.10Si$
1500 °C	$SiC_{0.33}O_{1.40}$	$SiC_{0.30}O_{1.40}+0.03C$	$SiC_{0.26}O_{1.42}$	$SiC_{0.26}O_{1.42}+0.03Si$	$SiC_{0.11}O_{1.57}$	$SiC_{0.11}O_{1.57}+0.10Si$

3.1.1. Density measurements

The density and SSA values of the powder samples for the systems T^H/D^H 1, 2 and 9 are reported in Table 2. Additionally, in Fig. 1, the density values are plotted as a function of the pyrolysis temperature between RT (gel-state) and 1500 °C. Starting from the gel, an increase of density with the T^H/D^H-ratio from 1 (1.26 g/cm^3), 2 (1.34 g/cm^3) up to 9 (1.54 g/cm^3) was found. This effect is related to the higher cross linking degree of T^H/D^H 9 compared to T^H/D^H 2 and 1 compositions.[17]

Also, at 400 °C, an increase of density in the gels was monitored. However, in the temperature range 400–1000 °C, the gels with the higher bonded carbon content (T^H/D^H 1 and 2) show a higher densification effect than T^H/D^H 9 and at 1000 °C the denser SiOC glass is the one derived from the T^H/D^H 1 gel. Above 1000 °C and up to 1500 °C density of T^H/D^H 1 (2.47±0.03 g/cm^3) and 2 (2.42±0.02 g/cm^3) maintain constant values. Density of T^H/D^H 9 is constant up to 1400 °C (2.270.03 g/cm^3) and slightly decreases from 1400 to 1500 °C (2.170.03 g/cm^3 at 1500 °C), probably due to the decomposition process of the oxycarbide phase.

3.1.2. SSA measurements

SSA values as a function of the pyrolysis temperature are reported in Table 2 and shown in Fig. 2. In gel state, T^H/D^H 9 revealed the highest specific surface area of ≈670 m^2/g. Increasing the temperature leads in linear decrease of the surface area that reaches a value close to zero at 1200 °C. At temperatures higher than 1200 °C the oxycarbide glass is dense. The C-rich samples show a reduced specific surface area in gel state (T^H/D^H 1 = 46 m^2/g; T^H/D^H 2 = 228 m^2/g). In the low temperature range (400–800 °C), first an increasing of the BET surface area due to organic/inorganic transformation reactions was found, followed by a reduction of surface area that can be related to a densification process. The development of this transient porosity during pyrolysis is a well known effect for all the polymer-derived ceramics and it is due to the evolution of gaseous compounds.[18] T^H/D^H 1 as well as T^H/D^H 2 show constant behaviour between 800 and 1200 °C with values of ≈40 m^2/g and ≈100 m^2/g, respectively. Above 1200 °C the surface area can be further reduced and at 1400 °C both oxycarbide glasses are dense.

Fig. 3 shows the general behaviour of the cumulative pore volume as a function of pore diameter for the

Table 2
Density and BET surface area for the studied oxycarbide glasses pyrolyzed in Ar (1 h) at temperatures between 400 and 1500 °C

Pyrolysis parameters	T^H/D^H 1		T^H/D^H 2		T^H/D^H 9	
	Density ρ (g/cm^3)	SSA±5% (m^2/g)	Density ρ (g/cm^3)	SSA±5% (m^2/g)	Density ρ (g/cm^3)	SSA±5% (m^2/g)
Gel	1.26±0.02	46	1.34±0.03	228	1.54±0.01	673
400 °C	1.44±0.02	271	1.56±0.02	364	1.75±0.02	458
600 °C	2.00±0.03	141	2.15±0.01	154	1.95±0.03	304
800 °C	2.26±0.02	43	2.32±0.02	119	2.17±0.02	219
1000 °C	2.45±0.02	39	2.41±0.01	108	2.24±0.02	117
1200 °C	2.46±0.01	32	2.43±0.03	94	2.27±0.01	0
1400 °C	2.48±0.03	4.6	2.40±0.01	0	2.27±0.03	0
1500 °C	2.49±0.02	0	2.41±0.02	0	2.17±0.03	0

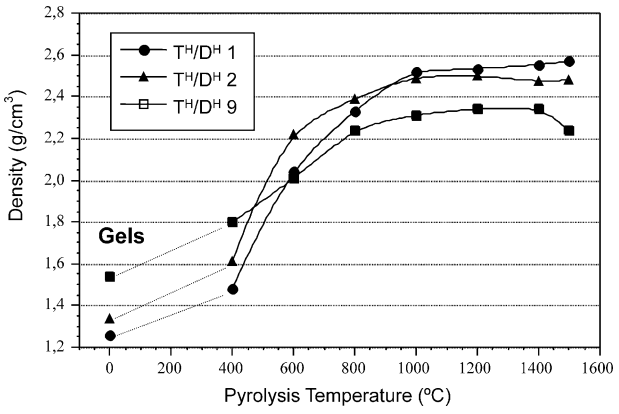

Fig. 1. Density values for the system T^H/D^H 1, 2 and 9, pyrolyzed in Ar-atmosphere (1 h) as a function of the pyrolysis temperature.

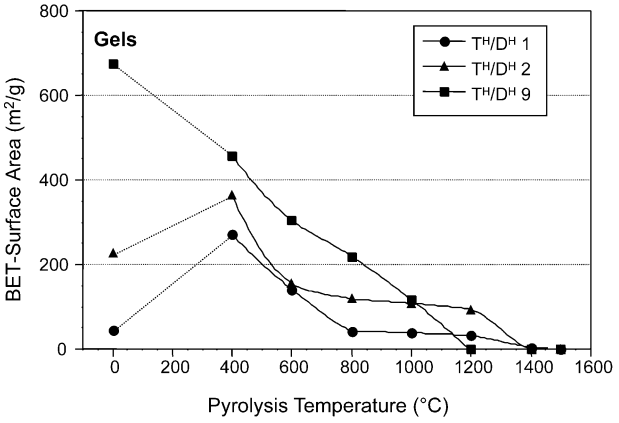

Fig. 2. BET surface area as a function of pyrolysis temperature in the system T^H/D^H 1, 2 and 9, pyrolyzed in Ar-atmosphere (1 h).

samples T^H/D^H 1, 2 and 9 at different pyrolysis temperatures. Most of the pores for the T^H/D^H 9 sample are below 100 Å while C-rich compositions (T^H/D^H 1 and 2) have larger pores above 100 Å. For the latter samples, the pyrolysis process up to 1000 °C leads to the closure of a large part of the finer porosity below 100 Å, but larger pores are still present up to 1200 °C. In order to have a fully densified material, temperature must be rised up to 1400 °C, when the BET-surface area drops to 0. This result suggests that the larger pores in the T^H/D^H 1 and 2 are closed by a viscous sintering process above the glass transition temperature of the SiOC-glasses, which is known to be in the range 1300–1350 °C.[19,20]

On the other hand, T^H/D^H 9 completely densifies at lower temperature (1200 °C), either due to the finer pores already present in the starting gel and for the lower amount of network carbon (see Table 1), which results in a lower viscosity material.

3.1.3. X-ray diffraction

The XRD patterns obtained from the glasses T^H/D^H 1, 2 and 9 after heat treatment in Ar-atmosphere at temperatures between 1200 and 1500 °C are reported in Fig. 4. The profile fitting and the Bragg's peak position of the expected phases SiO_2, SiC and Si are shown on each figure and for each composition as well as the experimental data points. The amorphous phase coming from the Si–O–C network is present for every composition and each pyrolysis temperature. Some features related to SiC are also visible even at the lowest temperature of treatment for each composition though the signal becomes really clear at 1400 °C. The pure silicon

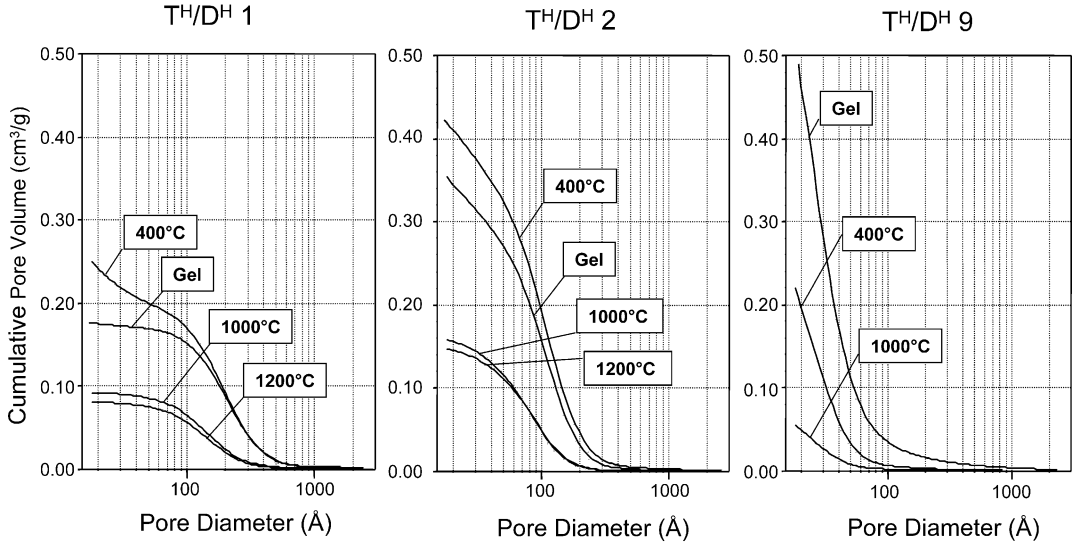

Fig. 3. Cumulative pore volume as a function of pore diameter at different pyrolysis temperatures in the systems T^H/D^H 1, 2 and 9, pyrolyzed in Ar-atmosphere (1 h).

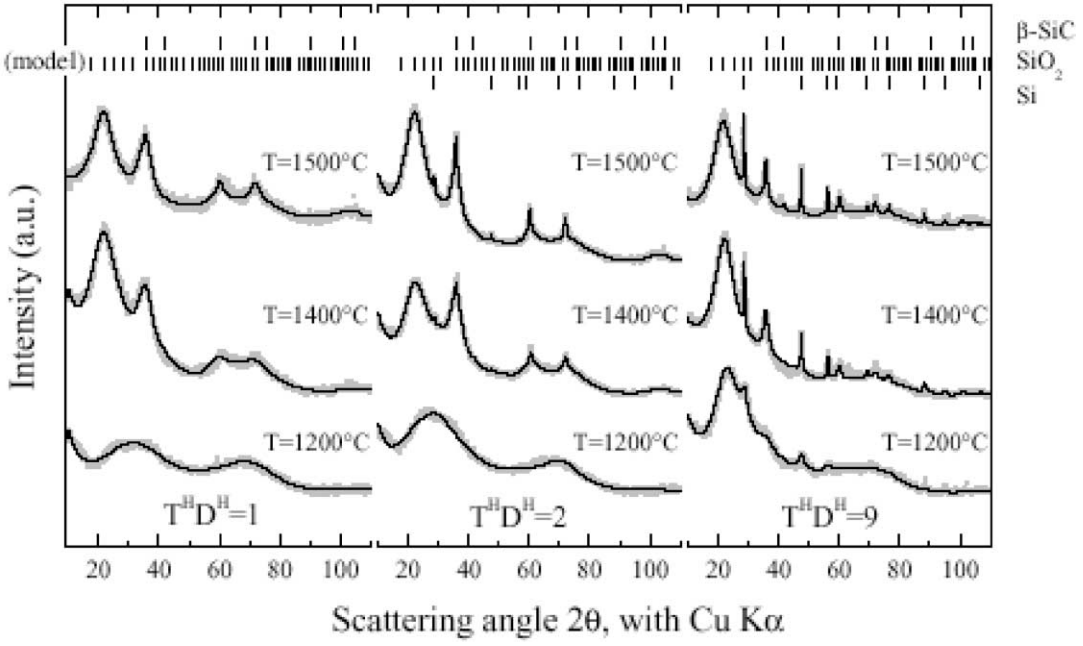

Fig. 4. XRD patterns recorded after pyrolysis at 1200, 1400 and 1500 °C of the system T^H/D^H 1, 2 and 9, pyrolyzed in Ar-atmosphere (1 h).

phase is detected in sample T^H/D^H 9 for each temperature but in sample T^H/D^H 2 it begins to be seen at 1400 °C. This phase is not present in the patterns of sample T^H/D^H 1.

The quantitative analysis and crystallite size calculated from the patterns are summarized for each composition in Table 3. It is noteworthy that these data should actually be regarded as semi-quantitative given the nature of approximations employed for our numerical approach. The evolution of the network with the temperature is different for each starting composition. Samples with excess of C (T^H/D^H 1) are amorphous at 1200 °C. The formation of β-SiC-nanodomains with a grain-size of ≈2nm takes place at 1400 °C. At 1500 °C their crystallite size is still around 2 nm suggesting a very slow growth rate. For T^H/D^H 2, β-SiC-nanodomains (1.5 nm) are visible at 1200 °C and their growth is comparable with the previous case (1.5 nm at 1400 °C and 3 nm at 1500 °C). Finally, in sample T^H/D^H 9 at 1200 °C, the formation of Si and SiC is observed. With increasing temperature both phases show an easier growth compared with the C-rich samples and at 1500 °C 16 nm SiC and ca 19 nm Si nanocrystals are present. These results agree with the idea that atom mobility in the SiOC network is reduced by the presence of C and therefore phase separation into SiO_2 and SiC, and thus the SiC formation is retarded in T^H/D^H 1 and 2 compared to T^H/D^H 9 sample.

3.2. Flexural strength analysis

The *MOR* and elastic modulus values of rod samples in the system T^H/D^H 1, 2 and 9 are reported in Table 4 and plotted as function of pyrolysis temperature in Figs. 5 and 7. In Fig. 5 the average *MOR* values are plotted as a function of pyrolysis temperature (600–1500 °C)

Table 3
Quantitative analysis and,crystallite size of T^H/D^H 1, 2 and 9 pyrolized in Ar (1 h) at 1200, 1400 and 1500 °C

	T^H/D^H 1		T^H/D^H 2			T^H/D^H 9		
	SiC (wt.%)	Amorph. phase (wt.%)	SiC (wt.%)	Si (wt.%)	Amorph. phase (wt.%)	SiC (wt.%)	Sp (wt.%)	Amorph. phase (wt.%)
1200 °C	–	100	5	0	95	4	4	92
1400 °C	16	84	27	1	72	8	2	90
1500 °C	30	70	12	1	87	6	4	90
	SiC		SiC	Si		SiC	Si	
1200 °C	–		1.0	–		1.5	2.5	
1400 °C	2.4		1.5	31.0		3.0	14.5	
1500 °C	1.8		3.0	30.0		16	19.2	
	Cryst. size (nm)		Cryst. size (nm)	Cryst. size (nm)		Cryst. size (nm)	Cryst. size (nm)	

Table 4
Modulus of rupture (*MOR*) and elastic modulus (*E*) area for studied oxycarbide glasses pyrolyzed in Ar (1 h) at temperatures between 400 and 1500 °C

Pyrolysis parameter	T^H/D^H 1		T^H/D^H 2		T^H/D^H 9	
	MOR (MPa)	*E* (GPa)	*MOR* (MPa)	*E* (GPa)	*MOR* (MPa)	*E* (GPa)
600 °C	53±13	15±2	61±20	34±3	67±16	18±1
800 °C	271±60	47±3	363±87	53±6	236±25	47±4
1000 °C	471±75	90±4	603±90	92±3	242±67	74±3
1200 °C			199±85	101±4	153±92	105±3
1400 °C			194±39	128±8	189±23	104±6
1500 °C			207±40	133±13	183±5	98±5

for the systems T^H/D^H 1, 2 and 9 pyrolysed in Ar-atmosphere. The mechanical strength data reveal a large scatter, reflecting a wide size distribution of critical defects. Beginning from 60 MPa at 600 °C, the oxycarbide glasses show an increase of *MOR* up to a maximum value of 600±90 MPa (T^H/D^H 2). The important increase of the *MOR* values between 600 and 1000 °C is certainly related to the conversion from an organic network into an inorganic SiOC material that it is known to occur in this temperature range.[21] *MOR* values at 800–1000 °C show a trend of increasing the fracture strength with the amount of MDES in the precursor gel and, in particular, the mechanical strength of oxycarbide glasses increases in the same way as the concentration of bonded carbon in the oxycarbide phase (see Table 1).[10] In the high temperature range (1000–1500 °C) a strong decrease of *MOR* down to values of ≈200 MPa is observed. This result accounts for the higher degree of surface and volume defects produced during firing and handling above 1000 °C., It is noteworthy to remind that for T^H/D^H 1 precursor gel it is impossible to pyrolyze crack-free samples above 1000 °C, probably due to the evolution of a higher amount of gaseous products (H_2) during pyrolysis.

The pyrolysation of T^H/D^H 2 samples at temperatures higher than 1300 °C, lead to the formation of longitudinal cracks along the rods, Fig. 6. This crack pattern implies the existence of a tangential tensile stress at the surface of the rod which could be associated to the earlier transformation (densification) of the surface compared to the core.

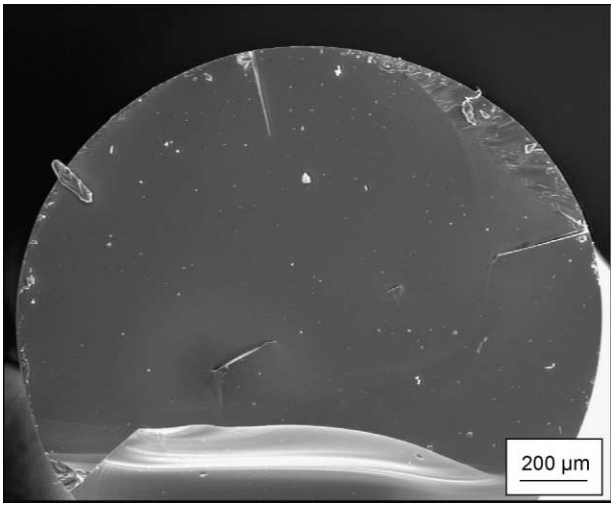

Fig. 6. SEM picture of the fracture surface of T^H/D^H2 pyrolyzed at 1400 °C in Ar-atmosphere (1 h) with the formation of longitudinal cracks.

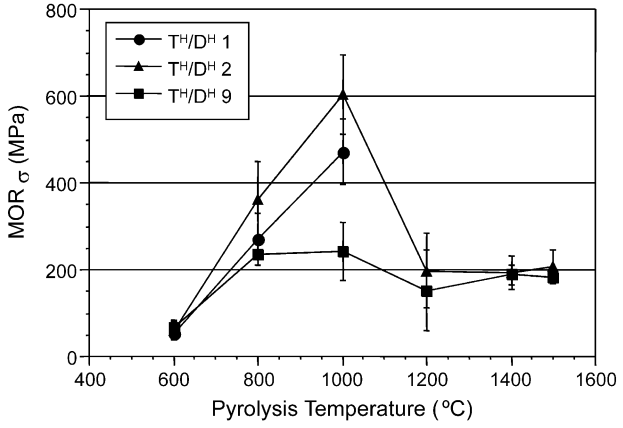

Fig. 5. Average *MOR* as a function of pyrolysis temperature in the system T^H/D^H 1, 2 and 9, pyrolyzed in Ar-atmosphere (1 h).

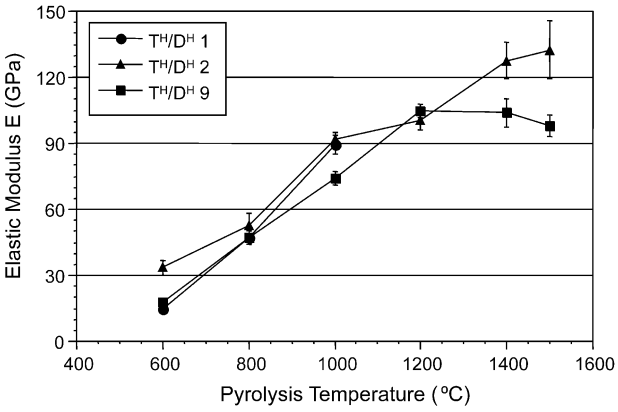

Fig. 7. Elastic modulus values as a function of pyrolysis temperature in the system T^H/D^H 1, 2 and 9, pyrolyzed in Ar-atmosphere (1 h).

3.3. Elastic modulus

In Fig. 7, the elastic modulus values of T^H/D^H 1, 2 and 9 are plotted as a function of the pyrolysis temperature. Starting from values of about 15 GPa for T^H/D^H 1 and 9 and 33 GPa for T^H/D^H 2 at 600 °C, the three compositions show a continuous increase of the elastic modulus with the pyrolysis temperature up to 1200 °C. Due to the damage of the T^H/D^H 1 samples during firing above 1000 °C, no high temperature data are available.

Remarkably high E values (90–130 GPa) for the system T^H/D^H 2 in the high temperature range between 1000 and 1500 °C have been recorded. Indeed, compared to SiO_2 glass ($E_{SiO_2} = 72$ GPa) SiOC glasses show an increase of E values from 25 to 80% in this temperature range.[10,22] T^H/D^H 9 precursor gel, that has the lowest C-content among the studied compositions, displays E values of ≈96 GPa (>37% compared to SiO_2) between 1200 and 1500 °C. Finally, at 1500 °C the T^H/D^H 9 system shows a decrease of the elastic modulus down to 100 GPa, attributed to the formation of bubbles in the core of the rods, Fig. 8. This can be explained by the production of gaseous SiO(g), which is formed from the reaction of free silicon ($Si_{(s)}$) and silica ($SiO_{2(s)}$) (3).

$$SiO_{2(s)} + Si_{(s)} \rightarrow 2SiO_{(g)} \quad (3)$$

Indeed, according to XRD measurements (see Table 3) and TEM analysis reported elsewhere[23] elemental, Si is formed in T^H/D^H 9 system at temperatures around 1200 °C. Above 1400 °C, nanodomains of silica and silicon react to form gaseous SiO and start to form bubbles, which are °well evident in the samples fired at 1500 °C (see Fig. 8).

The experimental data of the elastic modulus suggest that the two main parameters which control the elastic modulus are: (i) the amount of bonded carbon and (ii) the porosity of the samples. At 1400 °C, both the glasses are dense. The higher E value measured for T^H/D^H 2 (≈130 GPa) compared with T^H/D^H 9 (≈105 GPa) must be associated with the higher amount of substituted C in the glass structure, as shown by the CA or by the greater amount of crystalline SiC revealed by the XRD study. At 1200 °C, the elastic modulus of T^H/D^H 9 system is the same compared to 140 °C while T^H/D^H 2 shows a lower value (E≈100 GPa). Chemical composition of the samples is unaffected compared to 1400 °C, therefores the different values of elastic modulus must be associated with the different microstructure of the materials. A reasonable explanation could be that at 1200 °C, T^H/D^H 2 glass is still porous while T^H/D^H 9 is already dense.

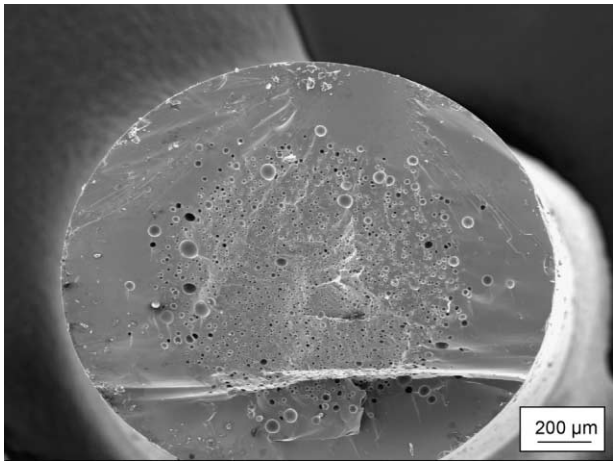

Fig. 8. SEM picture of the fracture surface of T^H/D^H9, pyrolyzed at 1500 °C in Ar-atmosphere (1 h) with the formation of bubbles.

3.4. Vickers hardness

Vickers hardness values are plotted in Fig. 9 and reported in Table 5 as a function of pyrolysis temperature in the range between 600 and 1500 °C in Ar-atmosphere. The indentations were performed on pyrolysed discs ≈5 mm in diameter and 1.5 mm thickness. The firing of thin slices is one possibility to produce crack-free oxycarbide glasses from T^H/D^H 1 gels at temperatures higher than 1000 °C.

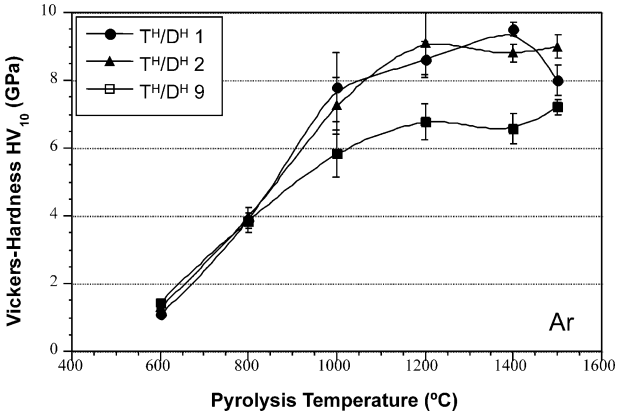

Fig. 9. Vickers hardness values as a function of pyrolysis temperature in the system T^H/D^H 1, 2 and 9, pyrolyzed in Ar-atmosphere (1 h).

Table 5
Vickers hardness (H_V) of T^H/D^H 1, 2 and 9 pyrolyzed in Ar (1 h) at temperatures between 400 and 1500 °C

Pyrolysis parameter	T^H/D^H 1	T^H/D^H 2	T^H/D^H 9
	$H_{V_{10}}$ (GPa)	$H_{V_{10}}$ (GPa)	$H_{V_{10}}$ (GPa)
600 °C	1.1±0.1	1.3±0.1	1.5±0.1
800 °C	3.9±0.4	4.0±0.1	3.9±0.2
1000 °C	7.8±1.0	7.3±0.9	5.8±0.7
1200 °C	8.6±0.5	8.4±1.0	6.8±0.5
1400 °C	9.5±0.2	8.8±0.3	6.6±0.5
1500 °C	8.0±0.5	9.0±0.4	7.2±0.2

Generally, the trend observed in the low temperature range (600–1000 °C) in Ar-atmosphere is similar to the already investigated density, *MOR* and *E* measurements. From 600 °C (1 GPa), the three oxycarbide glasses show a constant increase of H_V with similar values up to 800 °C (4 GPa) with a maximal standard deviation of 0.7 GPa, respectively. At higher temperatures, the stoichiometric compound T^H/D^H 2 reaches a value of ≈9 GPa which is retained up to 1500 °C. T^H/D^H 1 shows comparable values (≈9.5 GPa) and decreases (≈8 GPa) due to beginning of the decomposition reactions at 1500 °C. Higher T^H/D^H ratios, such as T^H/D^H 9, lead to a reduction of C in the network and form a silica rich system, which, in the temperarure range between 1200 °C and 1500 °C, displays a hardness of ≈6.5 GPa in good agreement with the values reported in the literature for fused silica glass ($H_{VSiO2} = 6.2$ GPa).

Optical (OM) and scanning electron (SEM) microscopy investigations have been performed with the aim of studying the mechanism of deformation under point loading.

3.4.1. T^H/D^H 1

Fig. 10a shows the optical micrograph of a Vickers indent, as well as the cross-section analysed by scanning electron microscopy (Fig. 10b), obtained with a load of 10 N on a T^H/D^H 1 sample pyrolyzed at 600 °C. The observed fracture pattern is typical for T^H/D^H 1 samples pyrolysed between 600 and 800 °C. It shows a Hertzian cone cracks which spread away from the surface at a characteristic angle (cone angle≈45°). The formation of Hertzian cone cracks is usually observed on a brittle material after contact with a hard blunt indent. However, when a sharp Vickers indent is loaded on the surface of fused silica or borosilicate glass, Hertzian cone cracks are also formed. For this reason these glasses are called anomalous[24] to distinguish them from the more conventional soda-lime glass[25] which forms, upon Vickers indentation, the classical radial-median and lateral cracks system. The anomalous behaviour under Vickers indentation of SiO_2 and SiO_2–B_2O_3 glasses compared to normal glasses is accounted for by a different mechanism responsible of the permanent deformation beneath the indenter. Accordingly, plastic deformation of anomalous glasses is mainly due to densification of the open SiO_2 and SiO_2–B_2O_3 network, while for the soda-lime glasses plastic deformation is elated to shear flow. These two different mechanisms of plastic deformation result into different contact stress fields which led to the different final crack patterns. Therefore, formation of circular cone cracks for T^H/D^H 1 pyrolyzed at 800 and 1000 °C, suggests that the deformation mechanism beneath the indentation is dominated by the densification of the Si–O–C network which behaves in the same way as pure silica. At temperatures between 1000 and 1200 °C, the indentation crack pattern of T^H/D^H 1 samples transforms into a mixture of cone crack and the more conventional radial/median and lateral systems (Fig. 11). At this temperature the cone angle (≈26°) approaches the typical value for silica, i.e. ≈22°.[26]

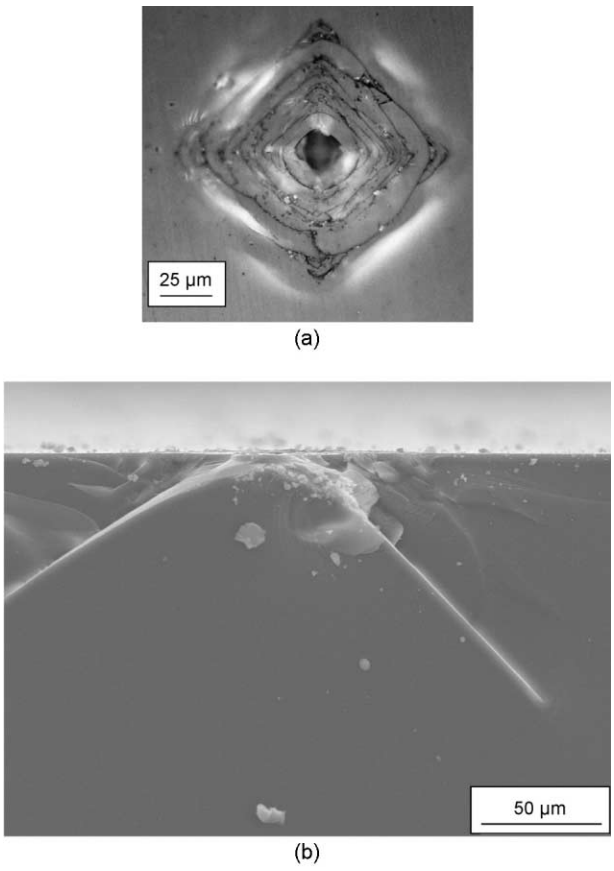

Fig. 10. (a) Typical optical micrograph of a Vickers indent (load 10 N) of T^H/D^H 1 at pyrolysis temperatures between 600 and 800 °C in Ar-atmosphere (1 h). (b) SEM picture (cross section) of a Vickers indent (load 10 N) of T^H/D^H 1 at pyrolysis temperatures between 600 and 800 °C in Ar atmosphere (1 h).

Between 1200 and 1500 °C, the radial/median and lateral crack systems are well developed (Fig. 12) however, cone cracks are still present up to the maximum temperature.

3.4.2. T^H/D^H 2

Hertzian cone cracks (cone angle≈45°) are also visible for T^H/D^H 2 samples in the temperature range between 600 and 800 °C, Fig. 13. In the temperature range between 1200 and 1400 °C the fracture pattern transforms into a mixture of cone crack and the more conventional radial/median and lateral systems. Finally, radial/median and lateral crack systems are well developed at 1500 °C. However, cone cracks (cone angle≈27°) are still present up to 1500 °C. The indentation behaviour of the stoichiometric compound is comparable with the T^H/D^H 1 but the transition from pure Hertzian cone cracks to a mixture of Hertzian and radial/median and lateral

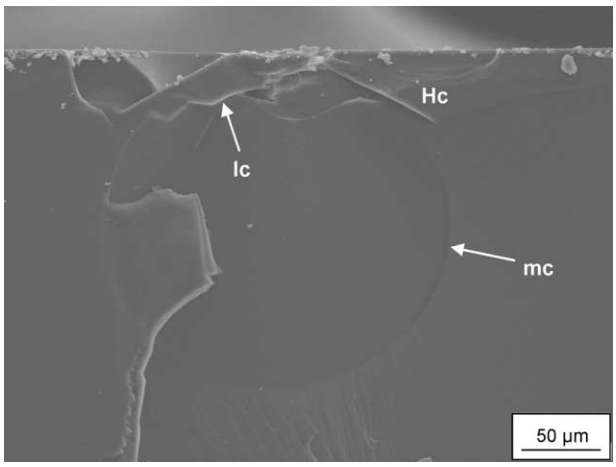

Fig. 11. SEM picture (cross section) of a Vickers indent (load 10 N) of T^H/D^H 1 at a pyrolysis temperature of 1000 °C in Ar-atmosphere (1 h).

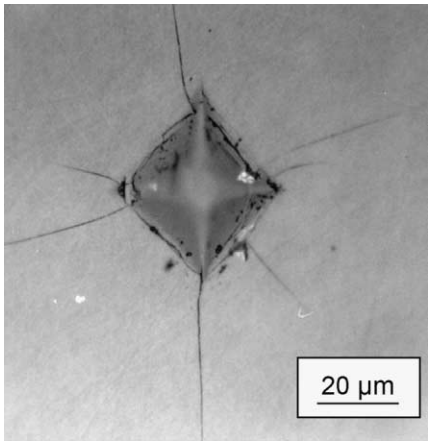

Fig. 12. Optical micrograph of a Vickers indent (load 10 N) of T^H/D^H 1 at at pyrolysis temperatures between 1200 and 1500 °C in Ar-atmosphere (1 h).

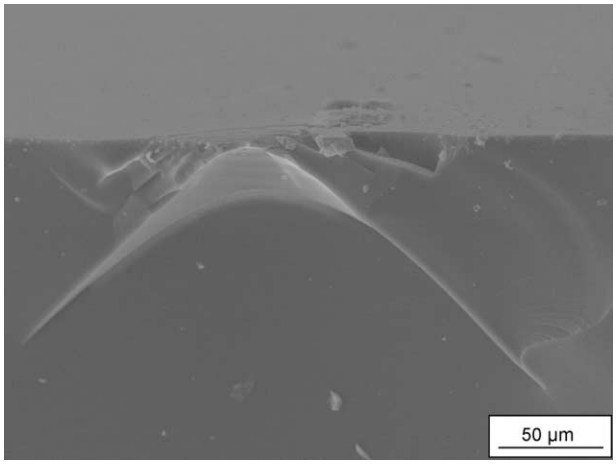

Fig. 13. SEM picture (cross section) of a Vickers indent (load 10 N) of T^H/D^H 2 at a pyrolysis temperature between 600 and 800 °C in Ar-atmosphere (1 h).

cracks is shifted about 200 °C toward higher temperatures (for the T^HD^H2 glass).

3.4.3. T^H/D^H 9

Finally, only Herztian cone cracks were found in the system T^H/D^H 9 pyrolysed from 600 to 1500 °C, Fig. 14. According to the low carbon content of this TREOS-rich precursor gel, the plastic deformation under the indenter is mainly due to a densification process and T^H/D^H 9 retains in the low as well as in the high temperature range his open structure like an anomalous glass. The cross-section of T^H/D^H 9 at 1400 °C (Fig. 14) clearly shows the deformation zone (dz) beneath the indentation site, the Herztian cone (Hc) (cone angle≈23°), the median/radial (rc) cracks and the lateral cracks (lc) beneath the plastic deformation zone.

At temperatures between 1200 and 1500 °C, in many cases the glass is shivered forming "volcano"-like structures, Fig. 15, which allow to clearly see the Hertzian cone cracks.

4. Discussion

By varying the T^H/D^H ratios from 1 to 9 it is possible to produce oxycarbide glasses with excess carbon (T^H/D^H 1), stoichiometric oxycarbide glasses with very low amount of C_{free} (T^H/D^H 2) and SiOC glass with free silicon (T^H/D^H 9). With increasing pyrolysis temperature, the composition of the oxycarbide glasses calculated from elemental analysis (Table 1) show a decrease of the C/Si ratio, while the corresponding O/Si ratio increases. Pycnometric analysis of the three glasses shows that their skeletal density is larger than pure silica (2.25 g/cm^3) beyond the experimental uncertainty. In particular, the values for T^H/D^H 1 and 2 (≈2.4–2.5 g/cm^3) are very close and quite different from T^H/D^H 9

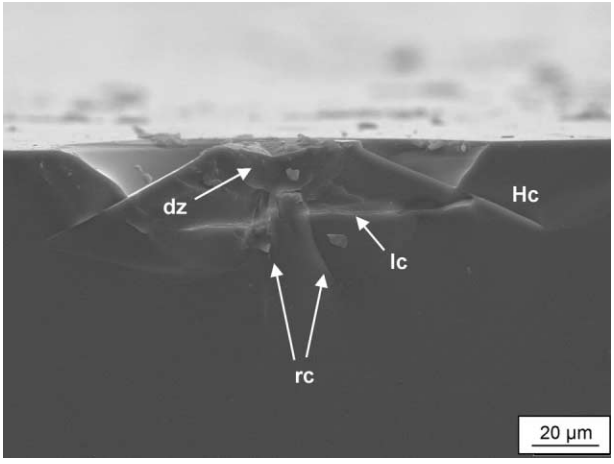

Fig. 14. SEM picture (cross section) of a Vickers indent (load 10 N) of T^H/D^H 9. The plastic deformation zone (dz), Hertzian cone (Hz), median/radial (rc) and lateral (lc) cracks are clearly visible.

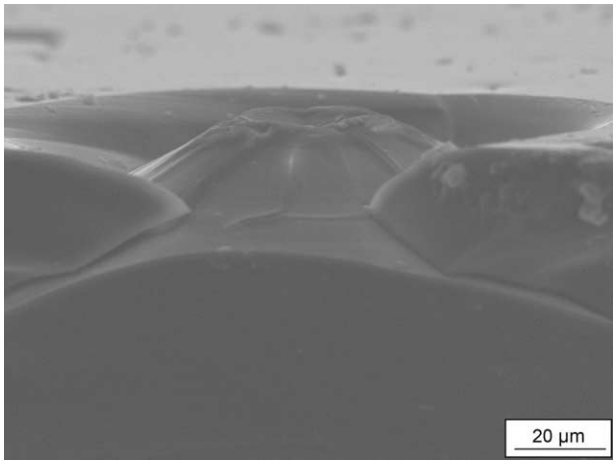

Fig. 15. SEM picture (cross section) of a Vickers indent (load 10 N) of T^H/D^H 9 at a pyrolysis temperature of 1400 °C in Ar atmosphere (1 h).

(≈2.3 g/cm^3). This suggests the occurrence of a more efficiently packed Si–C–O network in the former two C-rich specimens. The BET surface areas of the three glasses reduces to 0 at 1400 °C for T^H/D^H 1 and 2, but occurs earlier (1200 °C) for the T^H/D^H 9. According to the measurements of the cumulative pore volume, the pore elimination is observed to be easier in the specimen with the lowest carbon content, while in T^H/D^H 1 and 2 the larger pores are eliminated by a viscous sintering process between 1300 and 1400 °C.

The various microstructural characterization of the three oxycarbide glasses correlate well with the observed data of the mechanical properties. In the low temperature range between 600 and 1000 °C, the increase of density and reduction of BET surface area corresponds to a strong increase of the *MOR*, the elastic modulus and the Vickers hardness. The reason for this behaviour is certainly due to the mineralization reactions[21] which take place in the temperature range 600–1000 °C and lead to the insertion of carbon in the silica network via Si–C bonds, with a corresponding densification of the Si–O–C–(H) network. At higher temperature between 1000 and 1500 °C, the three oxycarbide glasses show different behaviour, mainly depending on the carbon inserted into the network, i.e. from the amount of Si–C bonds. This parameter influences the mechanical behaviour, either directly because it increases the average coordination number of the glass network, or indirectly because it increases the viscosity of the glass thereby shifting to high temperatures the formation of a dense material via viscous sintering.

T^H/D^H 2 samples reach *MOR* values of 600±90 MPa at 1000 °C and were controlled by surface defects at temperatures higher than 1200 °C. But the elastic modulus, as an intrinsic material property, increases with pyrolysis temperature. This behaviour agrees well with the decrease of the BET surface area and the closing of pores (>100 nm), due to viscous sintering at temperatures higher than 1350 °C. The elastic modulus values of the dense SiOC glasses, i.e. T^H/D^H 9 samples at 1200–1400 °C and T^H/D^H 2 pyrolyzed at 1400–1500 °C show an increase of ≈50% for T^H/D^H 9 and ≈100% for T^H/D^H 2 compared to pure silica (E_{SiO_2} = 60–65 GPa). Unfortunately, it was impossible to produce crack free samples from T^H/D^H 1 suitable for elastic modulus analysis at temperatures above 1000 °C. However, due to the higher amount of Si–C bonds present in this composition and previous measurements,[10] a higher elastic modulus is expected.

The Vickers hardness of T^H/D^H 1, 2 and 9 increase with the increase of the pyrolysis temperature in the range between 600 and 1000 °C, due to already mentioned increase of density as well as of the number of Si–C bonds (Table 1) in the silicon oxycarbide network. Between 1000 and 1500 °C, the values remain almost constant for T^H/D^H 9, whereas for T^H/D^H 1 and 2 further increases from 1000 to 1400 °C. This evolution can be easily correlated with the densification process which take place from 1200 to 1400 °C for T^H/D^H 1 and 2 while for T^H/D^H 9, a dense material is obtained at 1200 °C. The role of phase separation and crystallization of SiC and Si nano-crystals on the studied properties is more subtle. Indeed, in the classical field of glass ceramics, crystallization is usually accompanied by an increase of density and mechanical properties.[27] In the present case, nano-crystalline SiC and Si phases are formed in the temperature range between 1200 and 1500 °C. In the same range, the density of the materials is constant. This evidence could be explained thinking that the formation of crystalline SiC and Si occurs from SiC-rich amorphous regions of the same dimension (2–3 nm), through a short range diffusion process. Indeed, the presence of such amorphous SiC nano-domains in the SiOC glasses at temperature as low as 1000 °C has been recently shown by Kleebe et al.[7] Accordingly, the density change associated with this type of phase transformation should be negligible in agreement with the experimental findings. For the same reason also the mechanical properties of the SiOC glasses should be only slightly influenced by the crystallization process and the evolution of the elastic modulus and hardness in the 1000–1500 °C temperature range should be more related to the evolution of porosity, as has been already discussed.

Examination by OM and SEM of the Vickers impressions suggest that the fracture pattern induced by Vickers indentation is controlled by the amount of substituted carbon in the silicon oxycarbide network and the pyrolysis temperature. In particular Vickers indentation of SiOC glasses pyrolyzed at low temperature or with a low amount of substituted carbon preferentially deform by densification leading to the development of Hertzian cone craks, while radial cracks form at high temperature or for high value of substituted C. This

behaviour suggest that covalently bonded carbon atoms reduce the mobility of the network and therefore the deformation becomes less displacive (densification) and procede more by shear.

5. Conclusion

The characterization of mechanical properties was carried out on three silicon oxycarbide glasses with different substituted carbon loads pyrolyzed at various temperatures to evaluate the influence of these two parameters on flexural strength, elastic modulus Vickers hardness and impression patterns. The Si–O–C glasses obtained were respectively: (i) Si–O–C matrix with excess carbon, (ii) a stoichiometric compound ($SiC_xO_{2(1-x)}$, with $x=0.30$) and (iii) an oxycarbide matrix with excess of silicon. The glasses have been characterized with elemental analysis, density, BET and XRD techniques and compared with the mechanical properties. It has been found, that it is possible to produce nanocrystalline compounds with silicon carbide, silicon and excess carbon, which can be controlled in their microstructure within a narrow concentration range and appropriate choice of the starting precursor and subsequent thermal treatment. MOR, E and H_V increase with pyrolysis temperature and remarkably increase with an augmentation of the C/Si ratio, which correspond with the amount of SiC. This establishes a more efficiently packed Si–O–C network, which corresponds well with the indentation patterns of Vickers impression tests.

Acknowledgements

We would like to thank the European Commission who supported this work through the "Training and Mobility of Researchers (TMR) Program" (Contract FMRX-CT 98–0161).

References

1. Homeny, J., Nelson, G. G. and Risbud, S. H., Oxycarbide glasses in the Mg–Al–Si–O–C system. *J. Am. Ceram. Soc.*, 1987, **71**, 386–390.
2. Pantano, C. G., Singh, A. K. and Zhang, H. X., Silicon oxycarbide glasses. *J. Sol-Gel Sci. Technol.*, 1999, **14**, 7–25.
3. Babonneau, F., Thorne, K. and Mackenzie, J. D., Dimethyldiethoxysilane/tetraethoxysilane copolymers: precursors for the Si–C–O system. *Chem. Mater.*, 1989, **1**, 554–563.
4. Sorarù, G. D., Silicon oxycarbide glasses from gels. *Sol-Gel Science and Technology*, 1994, **2**, 843–848.
5. Corriu, R. J. P., Leclercq, D., Mutin, P. H. and Vioux, A., Si-29 nuclear-magnetic-resonance study of the structure of silicon oxycarbide glasses derived from organosilicon precursors. *J. Mater. Sci.*, 1995, **30**, 2313–2318.
6. Renlund, G. M., Prochazka, S. and Doremus, R. H., Silicon oxycarbide glasses: Part II. Structure and properties. *J. Mater. Res.*, 1991, **6**, 2723–2734.
7. Kleebe, J.-H., Turquat, C. and Soraru, G. D., Phase separation in a SiCO glass studied by transmission electron microscopy and electron energy-loss spectroscopy. *J. Am. Ceram. Soc.*, 2001, **84**, 1073–1080.
8. Sorarù, G. D., D'Andrea, G., Campostrini, R., Babonneau, F., Si–O–C glasses from gels. In *Proceedings of the International Symposium on Sol-Gel Science and Technology*, ed. The American Ceramic Society. 1995, pp. 135–146.
9. Sorarù, G. D., Sglavo, V. M., Dirè, S., D'Andrea, G. and Babonneau, F., High-strength, high-modulus silicon oxycarbide glasses. In *Proc. Third Euro-Ceramic Conference, 12–17 September 1993, Madrid, Spain, vol. 2*, ed. P. Duran and J. F. Fernandez. Faenza Editrice Iberica S. L, Spain, 1993, pp. 1157–1162.
10. Sorarù, G. D., Dallapiccola, E. and D'Andrea, G., Mechanical characterization of sol-gel derived silicon oxycarbide glasses. *J. Am. Ceram. Soc.*, 1996, **79**, 2074–2080.
11. Burns, G. T., Taylor, R. B., Xu, Y., Zangvil, A. and Zank, G. A., High-temperature chemistry of the conversion of siloxanes to silicon carbide. *Chem. Mater.*, 1992, **4**, 1313–1323.
12. Bois, L., Maquet, J., Babonneau, F. and Bahloul, D., Structural characterization of sol-gel derived oxycarbide glasses. 2. Study of the thermal stability of the silicon oxycarbide phase. *Chem. Mater.*, 1995, **7**, 975.
13. Babonneau, F., Soraru, G. D., D'Andrea, G., Dirè, S. and Bois, L., Silicon-oxycarbide glasses from sol-gel precursors. *Mater. Res. Soc. Symp. Proc.*, 1992, **271**, 789–794.
14. Sorarù, G. D., D'Andrea, G., Campostrini, R., Babonneau, F. and Mariotto, G., Structural characterization and high temperature behaviour of silicon oxycarbide glasses prepared from sol-gel precursors containing Si–H bonds. *J. Am. Ceram. Soc.*, 1995, **78**, 379–387.
15. Gregg, S. J. and Sing, K. S. W., *Adsorption, Surface Area and Porosity*. Academic Press, London, 1982.
16. Lutterotti, L., Ceccato, R., Dal Maschio, R. and Pagani, R., *Materials Science Forum*, 1998, **87**, 278–281.
17. Sorarù, G. D., D'Andrea, G., Campostrini, R. and Babonneau, F., Characterization of methyl-substituted silica gels with Si–H functionalities. *J. Mater. Chem.*, 1995, **5**, 1363–1374.
18. Riedel, R., Advances ceramics from inorganic polymers. In *Materials Science and Technology, A Comprehensive Treatment, Vol. 17B, Processing of Ceramics, Part II*, ed. R. J. Brook. VCH, Wurzburg, 1996, pp. 1–50.
19. Hammod, M., Breval, E. and Pantano, C. G., Microstructure and viscosity of hot pressed silicon oxycarbide glasses. *Ceram. Eng. Sci. Proc.*, 1993, **14**, 947–954.
20. Rouxel, T., Massouras, G. and Sorarù, G. D., High temperature behavior of an SiOC oxycarbide glass: elasticity and viscosity. *J. Sol-Gel Sci. Technol.*, 1999, **14**, 87–94.
21. Bois, L., Maquet, J., Babonneau, F., Mutin, H. and Balhhoul, D., Structural characterization of sol-gel derived oxycarbide glasses. I—study of the pyrolysis process. *Chem. Mater.*, 1994, **6**, 796–802.
22. Suyal, N., Krajewski, T. and Mennig, M., Sol-gel synthesis and microstructural characterization of silicon oxycarbide glass sheets with high fracture strength and high modulus. *J. Sol-Gel Sci. Technol.*, 1998, **13**, 995–999.
23. Turquat, C., Kleebe, H. J., Gregori, G., Walter, S. and Sorarù, G. D., TEM and EELS study of non-stoichiometric SiCO glasses. *J. Am. Ceram. Soc.*, in press.
24. Arora, A., Marschall, D. B., Lawn, B. R. and Swain, M. V., Indentation deformation/fracture of normal and anomalous glasses. *J. Non-Cryst. Sol.*, 1979, **31**, 415–428.
25. Hagan, J. T., Shear deformation under pyramidal indentations in soda-lime glass. *J. Mater. Sci.*, 1980, **15**, 1417–1424.
26. Lawn, B., *Fracture of Brittle Solids*. Cambridge University Press, Cambridge, UK, 1993.
27. McMillan, P. W., *Glass Ceramics*. Academic Press, London, UK, 1979.